Current Applied Physics 16 (2016) 31–36

Contents lists available at ScienceDirect

Current Applied Physics

journal homepage: www.elsevier.com/locate/cap

Quantum interference effects in chemical vapor deposited graphene

Nam-Hee Kim [a], Yun-Sok Shin [a, **], Serin Park [b], Hong-Seok Kim [a], Jun Sung Lee [a], Chi Won Ahn [c], Jeong-O Lee [b], Yong-Joo Doh [a, *]

[a] Department of Applied Physics, Korea University Sejong Campus, Sejong 339-700, Republic of Korea
[b] NanoBio Fusion Research Center, Korea Research Institute of Chemical Technology, Daejeon 305-343, Republic of Korea
[c] Nano-Materials Laboratory, National Nanofab Center, Daejeon 305-806, Republic of Korea

ARTICLE INFO

Article history:
Received 9 September 2015
Received in revised form
12 October 2015
Accepted 13 October 2015
Available online 22 October 2015

Keywords:
Graphene
Weak (anti)localization
Universal conductance fluctuations
Quantum interference

ABSTRACT

We report several quantum interference effects in graphene grown by chemical vapor deposition. A crossover between weak localization and weak antilocalization effects is observed when varying the gate voltage and we discuss the underlying scattering mechanisms. The characteristic length scale for phase coherence is compared with that estimated from universal conductance fluctuations in the micropore-formed graphene sample. These extensive temperature- and gate-dependent measurements of the intervalley and intravalley scattering lengths provide important and useful insight for the macroscopic applications of graphene-based quantum devices.

1. Introduction

Graphene [1], a monolayer honeycomb lattice of carbon atoms, provides a unique platform for studying two-dimensional relativistic quantum physics and for developing novel quantum-information devices. The half-integer quantum Hall effect [2,3] and Klein tunneling [4] were demonstrated in electrical-transport measurements, and graphene-based supercurrent transistors [5,6] and spintronic devices [7] were realized using mechanically exfoliated graphene. Recent advances in growth techniques of large-scale graphene films [8,9] by chemical vapor deposition (CVD) open the possibility of macroscopic applications of graphene-based quantum devices for integrated circuits. This provides a strong motivation for investigating the phase-coherent electronic-transport properties of CVD-grown large-scale graphene.

Previous studies of phase-coherent transport in graphene involved the magnetoconductivity (MC) measurement of exfoliated graphene flakes [10–14], which depends on inelastic and elastic scattering of charge carriers in graphene [15,16]. Since graphene exhibits a chiral nature, where the crystal momentum is coupled to the isospin due to a sublattice degeneracy, the backscattering of charge carriers is reduced. An unusual Berry phase of π is expected during coherent backscattering in each valley, resulting in destructive interference [15]. Thus, the weak antilocalization (WAL) in graphene results in negative MC curve [11]. When the sublattice degeneracy in graphene is broken by atomically sharp scatterers (e.g., sample edges or ridges), elastic intervalley scattering restores weak localization (WL), as evidenced by a positive MC [12,13]. Another type of elastic scattering is intravalley scattering due to ripples [16] and trigonal warping [15]; here, isospin is not conserved. Then, the effective time-reversal symmetry (TRS) is broken in each valley and WAL is suppressed [10,14].

In comparison with mechanically exfoliated graphene, there have been few MC measurements on CVD-grown graphene by varying temperature [17], or gate voltage [18], or strain [19], respectively. We here report an extensive study of phase-coherent electronic transport in CVD-grown and transferred large-scale graphene that shows clear gate-voltage and temperature dependences. The overall WL behavior is converted to the WAL feature near the charge-neutrality point (CNP) and the phase coherence length is compared with the one estimated from universal conductance fluctuations (UCFs) in graphene. Our observations provide important insight into quantum-electronic transport in CVD-grown and transferred graphene that is ultimately relevant for the development of novel quantum-information devices based on large-scale graphene.

* Corresponding author.
** Corresponding author.
E-mail addresses: yunsokshin@korea.ac.kr (Y.-S. Shin), yjdoh@korea.ac.kr (Y.-J. Doh).

http://dx.doi.org/10.1016/j.cap.2015.10.007
1567-1739/

2. Experiments

The growth and device-fabrication processes for graphene samples are illustrated in Fig. 1a–e. A Cu foil (10 × 10 mm^2) is mounted at the center of a quartz tube in a hot wall furnace under vacuum. After annealing the Cu foil at 1000 °C, graphene growth is initiated with a mixture of H_2 and CH_4 gases flowing through the quartz tube. After a continuous large-scale graphene film is formed on the Cu foil, the furnace is cooled down to room temperature (Fig. 1a). The graphene film is coated with a thin layer of polymethyl methacrylate (PMMA) and then it is baked at 120 °C to evaporate the solvent. The Cu foil is removed using a Cu etchant, leaving only the PMMA/graphene film (Fig. 1b). After the film is cleaned in a bath of deionized water, it is transferred onto a SiO_2/Si substrate (Fig. 1c). The PMMA film is removed with acetone, leaving the graphene layer on the SiO_2/Si substrate (Fig. 1d). A patterned film of Al is formed onto the graphene layer by photolithography and thermal evaporation of a 30-nm-thick Al film. The resultant pattern of Al/graphene film is formed by O_2 plasma etching of the graphene regions not masked by the Al film. After etching the Al film (etchant: AZ300 MIF), the patterned graphene is achieved (Fig. 1e). Three-terminal graphene devices contacted with Cr/Au (3 nm/15 nm) electrodes are fabricated by electron-beam lithography (Fig. 1f). Electrical transport properties are characterized in a two-point measurement configuration with and without a magnetic field (B), while a source-drain bias (V_{sd}) and a back-gate voltage (V_g) are applied.

After completion of the device fabrication, an atomic force microscopy (AFM) image and micro-Raman spectroscopy (532-nm laser excitation) results are compared directly to confirm the uniform thickness of the CVD-grown graphene film. The spatial map of the intensity ratio between the 2D (~2685 cm^{-1}) and the G (~1584 cm^{-1}) band Raman peaks, I_{2D}/I_G, gives values in excess of 2.0 over the entire graphene film in Fig. 2b, indicating uniform monolayer graphene [20]. Representative Raman spectra, obtained at three different locations on the film, are displayed in Fig. 2c. We note that the peak heights of the G band are almost the same, whereas those of the 2D band vary widely. The relatively large variation of I_{2D} is attributed to the spatially non-uniform adhesion between the transferred graphene and the substrate [21]. We also note that the disorder-induced D band (~1346 cm^{-1}) peak is very low or absent, reflecting the high quality of the CVD-grown graphene film [20].

3. Results and discussion

The temperature dependence of the sheet resistance R_{sheet} of the graphene sample is plotted in Fig. 2d as a function of V_g. It reveals that the charge neutrality point (or Dirac point) V_{CNP}, at which the electron and hole concentrations are equal, shifts from $V_g = 34.2$ V at room temperature to $V_g = 27.6$ V at $T = 2.6$ K. The carrier mobility and the mean free path at $T = 2.6$ K are estimated as $\mu = 1200\ (2000)\ cm^2/Vs$ and $l_m = 18\ (27)$ nm, respectively, for $\Delta V_g = -20\ (20)$ V, where $\Delta V_g = V_g - V_{CNP}$. These values are very similar to those obtained from a mechanically exfoliated graphene film [22]. The carrier concentration can be estimated from the relation [2] $n = 7.2 \times 10^{10}|\Delta V_g|\ (cm^{-2})$, which yields $n = 2 \times 10^{12}\ cm^{-2}$ for $|\Delta V_g| = 20$ V. In a strong magnetic field of $B = 9$ T, our graphene device exhibits conductance plateaus at $G = \nu e^2/h$ with $\nu = 2$ and 6, where e is the elementary charge and h is the Planck constant, as shown in the inset of Fig. 2d. Since the longitudinal conductivity is mixed with the Hall conductivity in a two-point measurement configuration [23], those plateaus are attributed to a "half-integer" quantum Hall effect [2,3], which is again indicative of single-layered graphene.

Fig. 3a shows the differential MC, $\Delta\sigma = \sigma(B) - \sigma(B = 0)$, at different temperatures under a fixed $V_g = 0$. We note that CVD-grown graphene displays positive MC, a typical feature of WL, and the positive MC correction clearly increases at lower temperatures. Quantitative analysis of the WL-induced conductivity correction is made possible by the theoretical formula derived by McCann et al. [15],

$$\Delta\sigma = \frac{e^2}{\pi h}\left[F\left(\frac{8\pi B}{\Phi_0 L_\phi^{-2}}\right) - F\left(\frac{8\pi B}{\Phi_0\left\{L_\phi^{-2} + 2L_i^{-2}\right\}}\right) - 2F\left(\frac{8\pi B}{\Phi_0\left\{L_\phi^{-2} + L_i^{-2} + L_*^{-2}\right\}}\right)\right]. \quad (1)$$

Here $F(z) = \ln(z) + \psi(0.5 + z^{-1})$, $\psi(x)$ is the digamma function, and $\Phi_0 = h/e$ is the magnetic-flux quantum. The characteristic length scales L_ϕ and L_i represent the phase-coherence length (or inelastic scattering length) and the elastic intervalley scattering length, respectively, while L_* means the elastic intravalley scattering length. The latter is given by $L_* = \sqrt{D\tau_*}$, where D is the diffusion constant and τ_* is the intravalley scattering time. Since $D = v_F l_m/2$,

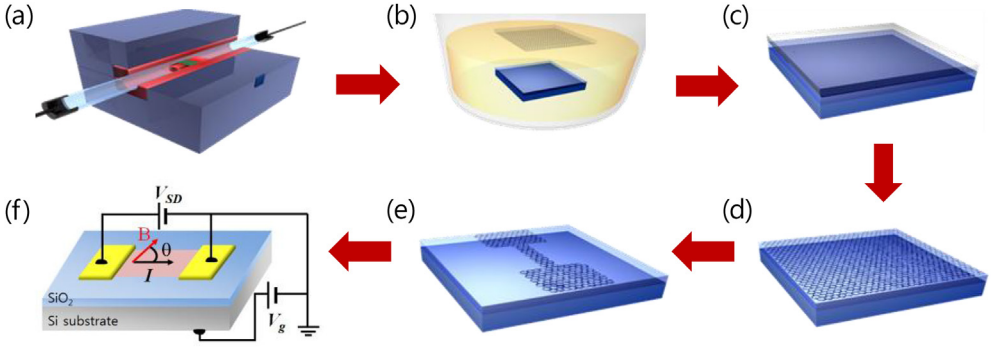

Fig. 1. Synthesis, transfer, and device fabrication processes for large-scale graphene film. (a) CVD growth of graphene film on a Cu foil (~10 × 10 mm^2). (b) Separation of a polymethyl methacrylate (PMMA)/graphene film from a Cu foil using a Cu etchant. (c) Transfer of PMMA/graphene film onto a SiO_2/Si substrate. (d) Removal of PMMA using acetone. (e) Micropatterning of a graphene film by oxygen plasma etching using an Al mask. The mask is removed with an Al etchant. (f) Deposition of metallic electrodes by electron-beam lithography and electron-beam evaporation. The source and drain electrodes are made of a Cr/Au double layer, while the highly doped Si substrate is used as a back gate. A magnetic field B is applied at various inclinations relative to the substrate.